Multicolored $Cd_{1-x}Zn_xSe$ quantum dots with type-I core/shell structure: single-step synthesis and their use as light emitting diodes†

Ying-Chih Pu and Yung-Jung Hsu*

We developed a single-step hot-injection process to synthesize $Cd_{1-x}Zn_xSe$ quantum dots (QDs) with tunable emission wavelengths. The multiple emission colors of the $Cd_{1-x}Zn_xSe$ QDs resulted from the variation in their compositions (x value) with the reaction time. Because of the higher reactivity of the Cd precursor, QDs whose composition was rich in CdSe were generated at the beginning of the reaction. As the reaction proceeded, the later-formed ZnSe shell was simultaneously alloyed with the core, giving rise to a progressive alloying treatment for the grown QDs. During the reaction period, the emission color of the $Cd_{1-x}Zn_xSe$ QDs shifted from red to orange, to yellow, to green and finally to blue. A light emitting diode (LED) composed of multilayers of ITO/poly(3,4-ethylenedioxythiophene):poly-(4-styrenesulfonate)/poly(3-hexylthiophene) blended with $Cd_{1-x}Zn_xSe$ QDs/Al was fabricated to test the electroluminescence (EL) properties of the QDs. The EL results show high color purity for the emission from LED devices containing $Cd_{1-x}Zn_xSe$ QDs, revealing that the as-synthesized QDs can be easily processed and integrated into a light-emitting device without using a complicated procedure. The findings from the present work also demonstrate the advantage of using the current single-step synthetic approach to obtain a batch of $Cd_{1-x}Zn_xSe$ QDs that may emit different colors in prototype LEDs.

Introduction

Quantum dots (QDs) have generated great fundamental and technical interest because of their novel tunable emission properties[1–5] and their potential applications in optoelectronic devices and biomedical tags.[6–12] It is possible to tune the bandgap rendering narrowband emission in the visible range for QDs by controlling their sizes.[13] QD based light emitting diodes (QD-LEDs) are of great interest for applications such as thin film displays with improved color saturation and high color rendering index (CRI) white lighting.[14–23] Since the first report on electrically driven QD-LEDs in 1994,[24] many studies have demonstrated that QD-LEDs can be fabricated by the combination of colloidal QDs with organic polymer and inorganic semiconductor layers. For example, Coe *et al.* designed a CdSe/ZnS red-emitting QD-LED through a phase-segregation technique that enabled the formation of a close-packed QD monolayer between an electron transport layer (ETL) and a hole transport layer (HTL) with a spin-casting step.[25] Sun's study demonstrated that different sizes of CdSe/ZnS QDs have

multicolor emission and that the different sizes can be utilized to fabricate QD-LEDs.[26] In Anikeeva's and Kwak's studies, QD-LEDs with tunable electroluminescence (EL) in the visible spectrum used different QDs as the active layer, such as ZnCdS/ZnS or $Cd_{1-x}Zn_xSe@ZnS$ in the blue, ZnSe/CdSe/ZnS or CdSe@ZnS in the green, CdSe/ZnS in the orange, and CdZnSe or CdSe/CdS/ZnS in the red range.[27,28] Bae *et al.* developed a layer-by-layer method to assemble green and yellow CdSe/ZnS QDs and orange and red CdSe/CdZnS/ZnS in all-QD multilayer films to fabricate QD-LEDs.[29] The all-QD multilayer films provided an exciton recombination zone within the QD-LEDs which may achieve multicolor EL from variously colored QDs. However, multicolored QD-LEDs must utilize QDs with different compositions or different sizes to obtain emission in different colors and must use a core/shell QD structure to acquire high quantum yields. For QDs with a core/shell structure, multistep and complicated synthetic methods are usually required to provide multicolor emission, which is elaborate and may hinder the applicability of the products. Therefore, creation of a technologically viable synthetic approach from which one could obtain multicolored core/shell QDs in a more effective manner is crucial to their practical utilization in solid-state lighting.

Ternary $Cd_{1-x}Zn_xSe$ QDs have received great attention because they have composition-tunable emission across the visible spectrum and are highly luminescent.[30] For instance, homogeneous $Cd_{1-x}Zn_xSe$ QDs could be prepared from a CdSe/ZnSe core/shell structure by an alloying process at a reaction

Department of Materials Science and Engineering, National Chiao Tung University, Hsinchu, Taiwan 30010, Republic of China. E-mail: yhsu@cc.nctu.edu.tw; Fax: +886 3 5724727; Tel: +886 3 5712121 ext. 55317

temperature above 270 °C, the alloying point.[31] The kinetics of the alloying mechanism involves the dissociation of Zn–Se bonds and the diffusion of Zn into CdSe. As the heating time increases, the blue-shift in the emission maximum of the spectra results from the progressive incorporation of the wider bandgap ZnSe shell into the CdSe core. Unlike the size-dependent photoluminescence (PL) of CdSe QDs, the bandgap of alloyed $Cd_{1-x}Zn_xSe$ QDs is tuned by the mole fraction of Cd/Zn. For $Cd_{1-x}Zn_xSe$ QDs with Cd mole fractions of 1 to 0.33, the first excitonic absorption and the PL spectra will gradually blue shift from the red to the blue region.

In this study, we developed a single-step hot-injection method to obtain alloyed $Cd_{1-x}Zn_xSe$ QDs with multicolor emission in the visible spectrum, and demonstrated the application of these alloyed QDs in QD-LEDs. The synthesis of $Cd_{1-x}Zn_xSe$ QDs that emitted red, orange, yellow, green and blue light was performed from precursors with a constant mole fraction (Cd/Zn = 1/9) at a high temperature, 320 °C, with progressive reaction times. We analyzed various $Cd_{1-x}Zn_xSe$ QDs by electron microscopy, UV-visible absorption, PL, and time-resolved PL spectroscopy, discussed the optical properties of the products, and illustrated that alloying may take place during particle growth and that the bandgap of $Cd_{1-x}Zn_xSe$ QDs will expand from 1.97 eV to 2.45 eV. Chemical etching results confirm that a thin shell of ZnS existed on the $Cd_{1-x}Zn_xSe$ QDs to form a type-I core/shell structure which confined the electrons and holes in the $Cd_{1-x}Zn_xSe$ core to provide stable PL. Moreover, we also demonstrated that in a multicolored QD-LED fabricated by a thin film process, $Cd_{1-x}Zn_xSe$ QDs synthesized in the current single-step process can act as the active emitting core in the device and show highly saturated EL.

Experimental section

Chemicals

Cadmium oxide (CdO, 99.99%), zinc acetate dihydrate (Zn(Ac)$_2$, 99.9%), selenium powder (Se, 99.9%), trioctylphosphine (TOP, 90%), oleic acid (OA, 90%), oleylamine (OLA, 90%), octadecene (ODE, 70%), benzylamine (BA), benzoyl peroxide (BPO) and poly(3-hexylthiophene) (P3HT) were used as purchased from Aldrich. Poly(3,4-ethylenedioxythiophene):poly(styrenesulfonate) (PEDOT:PSS) was used from Clevios PH500.

Synthesis of $Cd_{1-x}Zn_xSe$ QDs

Alloyed QDs of $Cd_{1-x}Zn_xSe$ were synthesized with a single-step hot-injection method. Typically, 0.1 mmol of CdO, 0.9 mmol of Zn(Ac)$_2$, 5 mL of OA, 5 mL of OLA and 5 mL of ODE were placed in a 100 mL round-bottom flask. The mixture was heated to 120 °C and degassed for 30 min, was filled with N$_2$ gas and was further heated to 320 °C to form a clear solution. 1.1 mmol of Se powder was dissolved in 1.5 mL of TOP in another 100 mL round-bottom flask to prepare TOP–Se. TOP–Se was also heated to 120 °C, degassed for 30 min and then heated under N$_2$ gas to 280 °C to form a clear solution. At these temperatures, 1.5 mL of TOP–Se was quickly injected into the reaction flask containing Cd–OA and Zn–OA. After the injection, the temperature of the reaction

flask was maintained at 320 °C to proceed the growth of $Cd_{1-x}Zn_xSe$ QDs. Aliquots of the sample were taken at different time intervals and were quenched in cold hexane to immediately terminate the growth of the particles. Ethanol was used to precipitate the resulting QDs in hexane, and the QDs were isolated by centrifugation. The excess ligand and reaction precursors were removed by extensive purification, and the QDs were redispersed in toluene for later characterization. The QD product obtained at the reaction time of 5 s, 1 min, 5 min, 15 min, 30 min, 60 min, and 90 min was respectively denoted as QD-5s, QD-1m, QD-5m, QD-15m, QD-30m, QD-60m, and QD-90m.

Characterization

UV-visible absorption spectra and PL spectra were obtained at room temperature with a Hitachi U-3900H spectrophotometer and a Hitachi F-4500, respectively. The excitation wavelength for PL measurement was set to 365 nm. Transmission electron microscopy (TEM) and high-resolution TEM (HRTEM) images were obtained with a JEOL JEM-2010 electron microscope operated at 200 kV. The particle size and size distribution of the QDs were also examined by dynamic light scattering (DLS) with the Malvern Zetasizer (Nano-ZS). The compositional information was obtained using energy dispersive spectrometry (EDS) with a field-emission scanning electron microscope (FESEM, Jeol, JSM-6500-F). Powder X-ray diffraction (XRD) patterns were acquired with a MAC Science MXP18 diffractometer with Cu Kα radiation (λ = 1.5405 Å) at 45 kV and 40 mA. Time-resolved PL measurements were performed in a time correlated single photon counting system (Pico Quant GmbH) which used a 375 nm picosecond pulsed diode laser (PDL-800-B, 20 MHz) as the excitation source. EL spectra of the QD-LEDs were measured using a StellarNet Black C-SR-25 spectrometer with F1000-UV-VIS-SR fiber optic cables. The applied bias and current density for EL measurement were 4.5 V and 50 mA cm^{-2}, respectively. Current–voltage (J–V) characteristics of the QD-LEDs were analyzed using a potentiostat (Jiehan-5600). To calculate the external quantum efficiency (EQE), the EL and J–V curves were measured simultaneously at the front side of the QD-LEDs. All the measurements were performed under atmospheric conditions and the devices were tested as-made without additional packaging.

Chemical etching of $Cd_{1-x}Zn_xSe$ QDs

Etching of the alloyed $Cd_{1-x}Zn_xSe$ QDs was performed with a scheme modified from a previous report by Chen and co-workers.[32] 0.5 mL of purified $Cd_{1-x}Zn_xSe$ QD solution was added to 1 mL of BA, and the mixture was sonicated for 30 min to exchange the surface ligand. Subsequently, 0.1 mL of the sonicated $Cd_{1-x}Zn_xSe$ QD solution was transferred to a solution of 0.8 mL of methanol and 1.2 mL of toluene. The etching solution was 0.2 M BPO in a toluene–methanol mixture (2 : 1 ratio by volume). Chemical oxidation of Cd, Zn and Se atoms on the QD surface might take place during the peroxide etching process, which results in the progressive dissolution of the QD surface. The oxidative etching process was initiated by the addition of etching solution and was stopped by the following purification process. The mixed solution was added to 10 mL of

methanol and was centrifuged for 3 min (8000 rpm) to remove the etching solution and the ions generated during the etching. The precipitate was redispersed in 2 mL of toluene, and the purification process was repeated twice. The purified precipitate was redispersed in toluene and was ready for UV-visible absorption, PL and TEM measurements.

Device fabrication

QD-LED devices with different emission wavelengths were fabricated as follows. Indium tin oxide (ITO) glass substrates were cleaned several times with ethanol and acetone and were used as the anode after UV/ozone (PSD-UV6 ozone system) treatment for 15 min. A PEDOT:PSS layer was spin-coated on the ITO surface at a spin rate of 4000 rpm for 30 s and was annealed at 150 °C for 30 min. A solution of 2 wt% P3HT:QDs was prepared by blending equal weight of P3HT and $Cd_{1-x}Zn_xSe$ QDs in chlorobenzene. The P3HT:QDs layer was spin-coated on PEDOT:PSS at 3000 rpm for 30 s and was annealed at 150 °C for 30 min. The cathode, the Al layer, was deposited by sputtering.

Results and discussion

The $Cd_{1-x}Zn_xSe$ QDs with tunable emission were synthesized by injecting TOP–Se into a solution at 320 °C. The solution contained a constant precursor ratio of $Cd : Zn = 1 : 9$ and oleic acid (OA) and oleylamine (OLA) surfactants in octadecene (ODE).
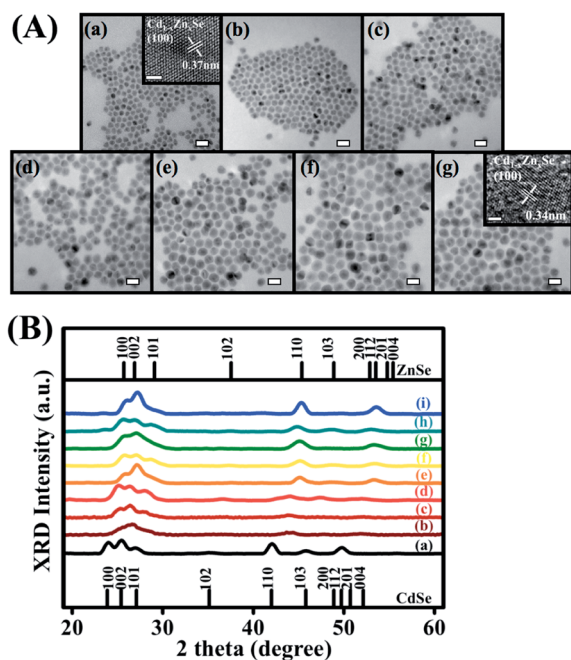

Fig. 1 (A) TEM images of $Cd_{1-x}Zn_xSe$ QDs at different reaction times: (a) 5 s, (b) 1 min, (c) 5 min, (d) 15 min, (e) 30 min, (f) 60 min and (g) 90 min. The inset is the corresponding HRTEM image. The scale bars of TEM images and HRTEM images are 20 nm and 2 nm, respectively. (B) XRD patterns of (a) pure CdSe QDs, (b–h) $Cd_{1-x}Zn_xSe$ QDs at different reaction times and (i) pure ZnSe QDs. The reaction times for the $Cd_{1-x}Zn_xSe$ QDs are (b) 5 s, (c) 1 min, (d) 5 min, (e) 15 min, (f) 30 min, (g) 60 min and (h) 90 min. The standard patterns of wurtzite CdSe and wurtzite ZnSe are included for reference.

Fig. 1 shows the TEM images of the $Cd_{1-x}Zn_xSe$ QDs at various reaction times. The size of the $Cd_{1-x}Zn_xSe$ QDs increased in the first half hour of the reaction, and then the size was maintained at approximately 15 nm until the reaction time reached 90 min; the sizes were 6.9 ± 1.1 nm (reaction time ∼5 s), 8.9 ± 1.2 nm (1 min), 12.3 ± 1.3 nm (5 min), 13.6 ± 1.4 nm (15 min), 15.1 ± 1.1 nm (30 min) and 15.2 ± 1.1 nm (90 min). At each reaction time, the $Cd_{1-x}Zn_xSe$ QDs possessed a spherical shape and a narrow size distribution, which reflects the high structural uniformity. The size variation of the QDs with the reaction time was consistent with the result of DLS measurement as shown in Fig. S1 (ESI).† Note that the hydrodynamic diameter determined from DLS was essentially larger than the apparent size from TEM because DLS resolved the entire ensemble of the QDs which included the surface-attached ligands.[33,34] The well-resolved lattice fringes of these fully crystalline QDs can be clearly seen in the insets of Fig. 1(A). An interlayer spacing of 0.36 nm was obtained for $Cd_{1-x}Zn_xSe$ QDs at 5 s of the reaction time; this spacing agrees well with the lattice spacing of the (100) planes of wurtzite CdSe. At the end of the reaction, the interlayer spacing of the $Cd_{1-x}Zn_xSe$ QDs decreased to 0.34 nm, which corresponds to the (100) planes of wurtzite ZnSe. The XRD data in Fig. 1(B) confirmed the crystalline wurtzite-type structure of the $Cd_{1-x}Zn_xSe$ QDs. Pure CdSe and ZnSe QDs were also synthesized by the same method, and their corresponding XRD patterns are compared in Fig. 1(B). It was found that the diffraction peaks of the $Cd_{1-x}Zn_xSe$ QDs gradually shift toward higher 2θ as the reaction time increases. The crystal structure of the $Cd_{1-x}Zn_xSe$ QDs after 5 s of reaction closely resembled pure CdSe QDs, and then the structure was transformed to that of pure ZnSe QDs after 90 min of reaction. Interestingly, during the QD growth process, the color of the reaction solution gradually changed from deep red to orange, to yellow, to green and then to blue. Fig. 2 shows the UV-visible absorption and PL spectra of $Cd_{1-x}Zn_xSe$ QDs at different reaction times. As the reaction time of the $Cd_{1-x}Zn_xSe$ QDs increased from 5 s to 90 min, a significant blue shift of about 100 nm was observed for both the onset of the first excitonic absorption (1S transition, $1S(e)–1S_{3/2}(h)$)[35] and the band edge of the PL peak of the QDs. As the reaction time increased from 5 s to 1 min, 5 min, 15 min, 30 min, 60 min, and 90 min, the corresponding PL peak shifted from $\lambda = 629$ to 620, 613, 593, 569, 531, and then 506 nm. The PL emission from these $Cd_{1-x}Zn_xSe$ QDs spanned the visible spectrum from the red to the blue, and the Gaussian-shaped PL peak had a full width at half-maximum (FWHM) narrower than 35 nm. The PL quantum yield (QY) of the $Cd_{1-x}Zn_xSe$ QDs was further determined from eqn (1):[36a,b]

$$QY = QY_{st} \left(\frac{A_{st}}{A_s} \right) \left(\frac{D_s}{D_{st}} \right) \left(\frac{n_s^2}{n_{st}^2} \right) \qquad (1)$$

QY_{st} is the quantum yield of a standard substance, quinine sulfate, and is known to be 54% in a 0.1 M H_2SO_4 solution with excitation at 310 nm.[36c] A_{st} and A_s are the absorbance values of the quinine and $Cd_{1-x}Zn_xSe$ QD samples at wavelengths of 310 and 365 nm, respectively. D_s and D_{st} are the corresponding integrated PL intensities for the $Cd_{1-x}Zn_xSe$ QD samples and quinine, respectively (the excitation wavelengths were 365 nm and 310 nm for the $Cd_{1-x}Zn_xSe$ QDs and quinine, respectively).
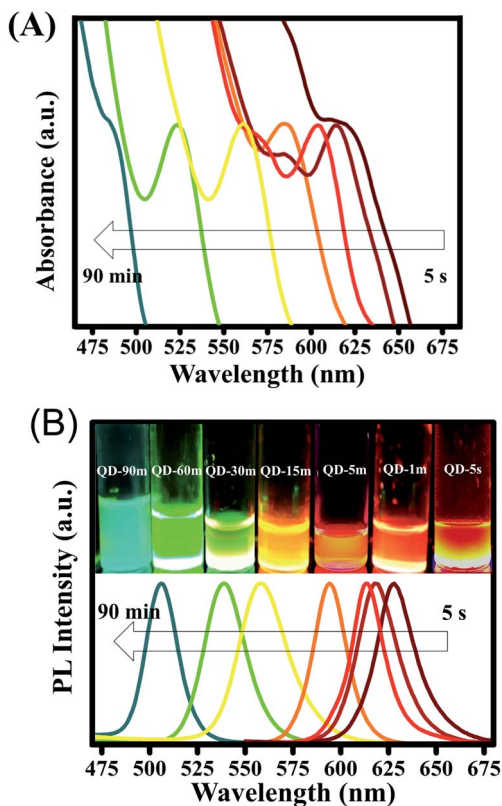
Fig. 2 (A) UV-visible absorption and (B) PL (with $\lambda_{ex} = 365$ nm) spectra for $Cd_{1-x}Zn_xSe$ QDs at reaction times of 5 s, 1 min, 5 min, 15 min, 30 min, 60 min and 90 min. The inset is a photograph of $Cd_{1-x}Zn_xSe$ QDs emitting different colors upon irradiation with a UV lamp.
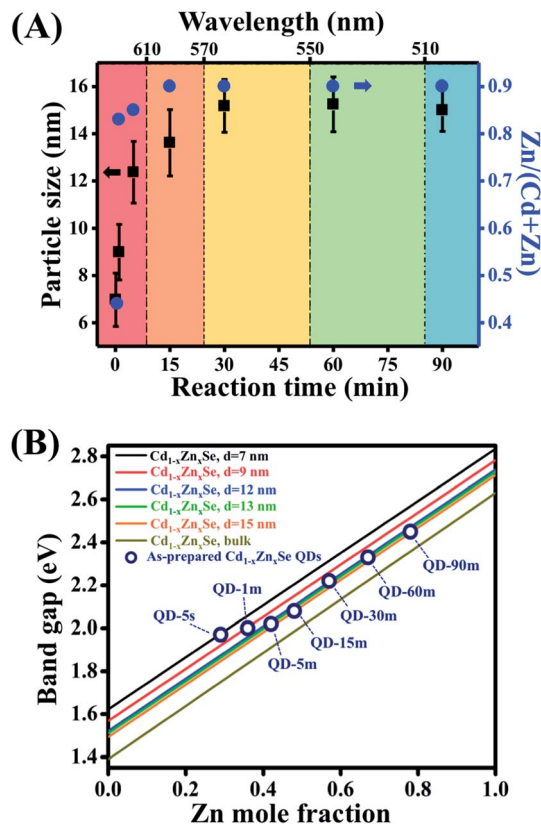

Fig. 3 (A) The compositions and particle size distributions of $Cd_{1-x}Zn_xSe$ QDs corresponding to emission wavelengths at different reaction times. (B) The dependence of the bandgap on composition for $Cd_{1-x}Zn_xSe$ QDs with particle sizes from 7 to 15 nm and bulk $Cd_{1-x}Zn_xSe$.

n_s and n_{st} are the refractive indices of the solvents used ($n_s = 1.49$ for toluene and $n_{st} = 1.33$ for H_2O). The room temperature PL QY for $Cd_{1-x}Zn_xSe$ QDs with different emission decreased gradually from red to blue as the reaction proceeded. The determined QY was 31%, 30%, 30%, 28%, 23%, 13% and 1% for QD-5s, QD-1m, QD-5min, QD-15m, QD-30m, QD-60m and QD-90m samples, respectively.

QDs were nanoscale particles and the sizes of these particles determined the emission wavelengths, as in pure CdSe QDs. When the particle size of CdSe increased from 2 nm to 4 nm, the emission wavelength red shifted from 530 nm to 630 nm.[37] Fig. S2 and S3 (ESI)† show the TEM images, UV-visible absorption and PL spectra of pure CdSe QDs, in which the red shifts of absorption and PL spectra correspond to increases in particle size. However, the emission properties of the alloyed QDs were not only influenced by size but also by composition.[38] Here we investigated the effects of size and composition on the emission of $Cd_{1-x}Zn_xSe$ QDs. Fig. 3(A) integrates the relationships between reaction time, emission wavelength, particle size and composition for the $Cd_{1-x}Zn_xSe$ QDs. From the TEM results, the particle size of the $Cd_{1-x}Zn_xSe$ QDs increased from 7 nm to 15 nm in the first 30 min and then was approximately 15 nm until the end of the reaction. At the same time, the atomic ratio of Zn as measured by EDS also increased and then was 90% from 30 to 90 min. The emission wavelength change of the $Cd_{1-x}Zn_xSe$ QDs was distinct from that of pure CdSe QDs,

even as the particle size increased. As the reaction progressed, a blue shift in the emission wavelength from 629 nm to 506 nm was observed for $Cd_{1-x}Zn_xSe$ QDs. This phenomenon suggested that the grown $Cd_{1-x}Zn_xSe$ QDs were progressively alloyed nanocrystals with an emission band edge dependent on composition.

For quantum-confined alloyed nanocrystals of $Cd_{1-x}Zn_xSe$, the dependence of the bandgap energy, E_g, on alloy composition (x) and particle diameter (d) can be described by eqn (2).[39]

$$E_g^{alloy}[d, x] = \left(E_{g,\infty}^{CdSe} + \frac{1.83}{d^{1.06}}\right)(1-x) + \left(E_{g,\infty}^{ZnSe} + \frac{2.08}{d^{1.19}}\right)x - bx(1-x) \quad (2)$$

$E_{g,\infty}^i$ is the bulk bandgap for i = CdSe or ZnSe ($E_{g,\infty}^{CdSe} = 1.74$ eV, $E_{g,\infty}^{ZnSe} = 2.63$ eV), and b is the bowing parameter, which is 0.35 for $Cd_{1-x}Zn_xSe$. According to eqn (2), the relationship between the Zn composition and the bandgap of the alloyed $Cd_{1-x}Zn_xSe$ nanocrystals with different particle sizes was depicted in Fig. 3(B). A linear relationship was observed not only in the QD system, but also in the bulk system. In addition, the composition of the $Cd_{1-x}Zn_xSe$ QD samples can be determined from the particle size and the PL wavelength using eqn (2). As shown in Fig. 3(B), the Zn compositions, x, of the $Cd_{1-x}Zn_xSe$ QDs were

0.29, 0.36, 0.42, 0.48, 0.57, 0.67 and 0.78 for QD-5s, QD-1m, QD-5m, QD-15m, QD-30m, QD-60m and QD-90m, respectively. The Zn compositions of the $Cd_{1-x}Zn_xSe$ QDs were also measured by EDS, and the results were 0.44, 0.83, 0.85, 0.9, 0.9, 0.9 and 0.9 for QD-5s, QD-1m, QD-5m, QD-15m, QD-30m, QD-60m, and QD-90m, respectively. The differences between the measured and calculated values signify that the present $Cd_{1-x}Zn_xSe$ QDs were not merely composed of single-phase $Cd_{1-x}Zn_xSe$. Since the Zn compositions from the EDS results were higher than those calculated from eqn (2), we suggested that the $Cd_{1-x}Zn_xSe$ QDs had a core/shell structure in which the core was alloyed $Cd_{1-x}Zn_xSe$ and the shell was ZnSe.

The suggested core/shell structure of the QD products was further confirmed with the chemical etching experiment in which peroxide was used to etch the QD surface.[32,40–42] The surface etching process can be realized through the variation of the absorption spectrum. For a single-phase structure such as pure CdSe QDs, the absorption spectrum blue shifts as the particle size decreases through oxidative etching; besides, a smooth decrease pattern is observed in the absorbance as the QDs tested were compositionally homogeneous. In contrast, for a core/shell type structure, an abrupt turning point, a "phase shift", would be observed in the first excitonic absorption due to the different etching rates at the shell and core composition.[40] Particularly, for the type-II core/shell structure, a blue shift in the first exciton absorption was accompanied during chemical etching, as in the case of CdSe/CdTe.[41] As to the type-I core/shell structure like CdSe/ZnS, the wavelength of the first exciton absorption remains unchanged with chemical etching.[42] In this work, we monitored the absorption spectrum and the PL transformation for QD-1m and QD-60m samples during the chemical etching process. As displayed in Fig. S4 (ESI),† the first excitonic absorption of the $Cd_{1-x}Zn_xSe$ QDs decreased in intensity but did not shift after chemical etching, and the PL emission also decreased in intensity after etching but did not shift. The inset TEM images in Fig. 4(A) clearly show that upon etching, the size of the $Cd_{1-x}Zn_xSe$ QDs decreased and the size distribution was preserved. The PL intensity of QD-1m declined to 40% after 90 s of chemical etching and to 3.5% after 240 s of etching. For QD-60m sample, the PL depression was much faster, reaching 0.7% after 90 s of chemical etching. Note that the PL of core/shell QDs is highly related to the interfacial properties such as surface states and shell thickness. Here the observed PL depression of the $Cd_{1-x}Zn_xSe$ QDs upon chemical etching was ascribed to the generation of structural defects at the particle surface or interface as the shell was etched. On the other hand, a "phase shift" in the first excitonic absorption was observed during the chemical etching of the alloyed QDs. As shown in Fig. 4(B), an abrupt point was noticed during chemical etching, which manifests the existence of a core/shell structure for the $Cd_{1-x}Zn_xSe$ QDs. The PL depression of the $Cd_{1-x}Zn_xSe$ QDs without a wavelength shift during chemical etching illustrates that the core/shell structure was type-I and that the etching generated structural defects on the particle surface. The surface defects may trap the photoexcited charge carriers to suppress the resultant PL. Moreover, the rate of PL depression during chemical etching for QD-60m was faster than that for
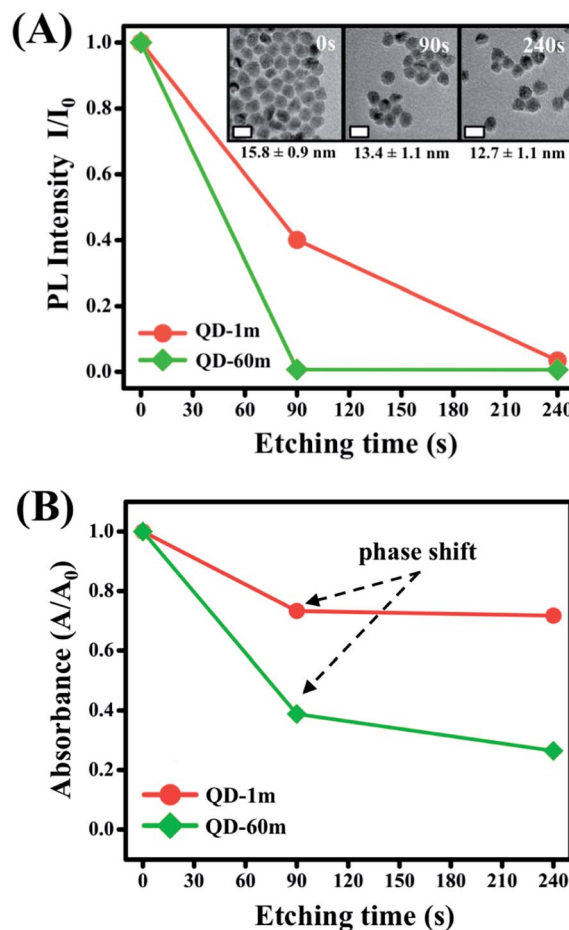

Fig. 4 (A) PL intensity (I/I_0) as a function of chemical etching time for $Cd_{1-x}Zn_xSe$ QDs, QD-1m and QD-60m. The insets are TEM images of QD-60m during the etching process showing the reduction in particle size. The scale bar of the insets was 20 nm. (B) UV-visible spectral transition of etched $Cd_{1-x}Zn_xSe$ QDs at 605 and 516 nm for QD-1m and QD-60m, respectively.

QD-1m, as can be clearly seen in Fig. 4(A). Since QD-1m was obtained at the initial stage of reaction, it was supposed to have a relatively thicker ZnSe shell than QD-60m, which leads to the more sustainable PL as the passivation shell was etched.

To characterize the optical quality of the different colored $Cd_{1-x}Zn_xSe$ QDs, we performed time-resolve PL measurement at the corresponding emission maxima of the samples. Because QD-5s, QD-1m and QD-5m all emitted lights in the red-colored region, one of them was chosen to further characterize the red emission of the QDs. Fig. 5 represents the time-resolved PL spectra for five representative $Cd_{1-x}Zn_xSe$ QD samples, QD-1m (red), QD-15m (orange), QD-30m (yellow), QD-60m (green), and QD-90m (blue). These spectra were analyzed with triexponential kinetics which generated three decay components (τ_1, τ_2, and τ_3) respectively assigned to exciton radiative recombination, quenching processes by the local environment, and carrier trapping at defect states.[43] The intensity-average lifetime ($\langle\tau\rangle$) was then calculated to make an overall comparison of the exciton fate. As Table 1 shows, a progressive decrease in the PL lifetime was noticed from QDs with red emission to QDs with
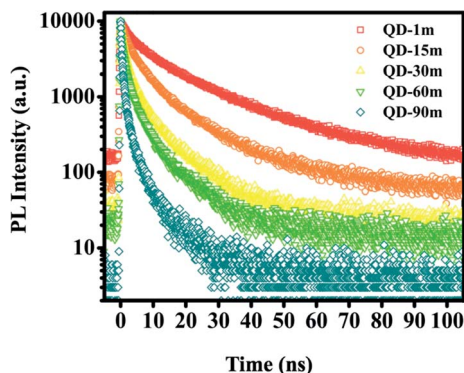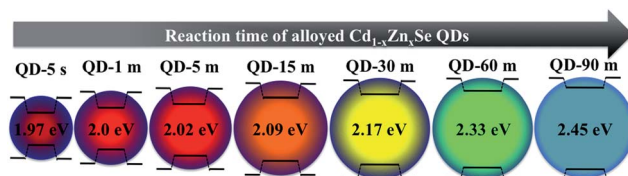
Fig. 5 Time-resolved PL spectra for $Cd_{1-x}Zn_xSe$ QDs at different reaction times.

Scheme 1 Plausible growth mechanism for $Cd_{1-x}Zn_xSe$ QDs. Because of the reactivity difference between the Cd and Zn precursors, QDs with a Cd-rich core were first formed; this formation was followed by the diffusion of ZnSe into the core and the alloying of ZnSe with CdSe. This alloying led to an increase in the bandgap of the QDs such that a blue shift of the PL emission was observed even for larger sized QDs.

blue emission. The average emission lifetime of QD-1m, QD-15m, QD-30m, QD-60m, and QD-90m was 19.0, 10.9, 6.2, 4.7, and 2.4 ns, respectively. This lifetime shortening was consistent with the progressive decrease in QY observed for these samples. The gradually shorter PL lifetime was attributed to the increasingly pronounced nonradiative relaxation of QDs arising from surface defects or lattice strain created in the progressive alloying process.[44,45] The significantly enhanced amplitude contribution from the fastest decay component (A_3) and its dominance over the slow decay term (A_1) may support the above proposition.

A plausible mechanism for the growth and the accompanying PL wavelength shift of the $Cd_{1-x}Zn_xSe$ QDs was proposed and is illustrated in Scheme 1. Note that the Zn precursor, Zn–OA, has a higher bond energy (71 kcal mol^{-1} for Zn–O bonding) and thus a lower reactivity than the Cd precursor of Cd–OA (57 kcal mol^{-1} for Cd–O bonding).[46,47] Because of this reactivity difference, QDs whose composition was rich in CdSe were generated at the beginning of reaction. As the reaction proceeded, the later-formed ZnSe shell was simultaneously alloyed with the core, giving rise to a progressive alloying treatment for the grown QDs. In the current synthetic system, OLA played a critical role in inducing the significant PL shift (of about 100 nm) for the $Cd_{1-x}Zn_xSe$ QDs during the reaction period. It should be mentioned that a comparative synthesis conducted without the addition of OLA showed only approximately 25 nm of the PL shift for the grown QDs, as displayed in Fig. S5 (ESI).† It has been reported that the amine molecules could attack the carbonyl group to release Zn from Zn–OA and promote the growth of ZnSe.[48] In the current synthesis, the employment of

OLA not only facilitated the ZnSe growth but also promoted the alloying within the $Cd_{1-x}Zn_xSe$ QDs. When TOP–Se was injected into the mixed solution of Cd–OA and Zn–OA, the presence of OLA activated Cd–OA and Zn–OA to release Cd and Zn and form alloyed $Cd_{1-x}Zn_xSe$ QDs. The nucleation was driven by Cd and Se because of the higher reactivity of Cd–OA; as a result, Cd-rich $Cd_{1-x}Zn_xSe$ cores were formed with ZnSe shells. As the reaction progressed, the QD size increased from 7 nm to 15 nm and the bandgap expanded from 1.97 eV to 2.17 eV, signifying that the particle growth and shell alloying simultaneously took place. From 30 to 90 min, the particle size remained 15 nm, while the bandgap expanded further to 2.45 eV, implying that this process should be dominated only by alloying.

With the type-I core/shell structure which can efficiently confine electrons and holes in the core, the present $Cd_{1-x}Zn_xSe$ QDs may find promising potential in luminescence applications. Particularly, the presence of the ZnSe shell enabled these alloyed QDs to retain their PL after being precipitated or even redispersed in the solid state, which makes the $Cd_{1-x}Zn_xSe$ QDs a practical active layer in LEDs. To assess the applicability, we fabricated a prototype QD-LED by utilizing a conductive polymer, poly(3-hexylthiophene), blended with $Cd_{1-x}Zn_xSe$ QDs (denoted as P3HT:QDs) as the active layer. As illustrated in Fig. 6(A), the QD-LEDs comprised the multilayer structure of ITO/PEDOT:PSS/P3HT:QDs/Al. Fig. S6 (ESI)† shows the TEM image of the P3HT:QD layer, which reveals considerably good dispersion of QDs within P3HT. To ensure carrier recombination within the $Cd_{1-x}Zn_xSe$ QDs, P3HT and PEDOT:PSS were chosen as the ETL and the HTL, respectively. The ETL and HTL employed not only provided high electron and hole mobility,[9,49,50] but also exhibited compatible energy levels for generating EL purely from the QDs. As shown in Fig. 6(B), QD-LEDs that contained different $Cd_{1-x}Zn_xSe$ QDs may emit

Table 1 Kinetic analysis of emission decay for $Cd_{1-x}Zn_xSe$ QDs at different reaction times

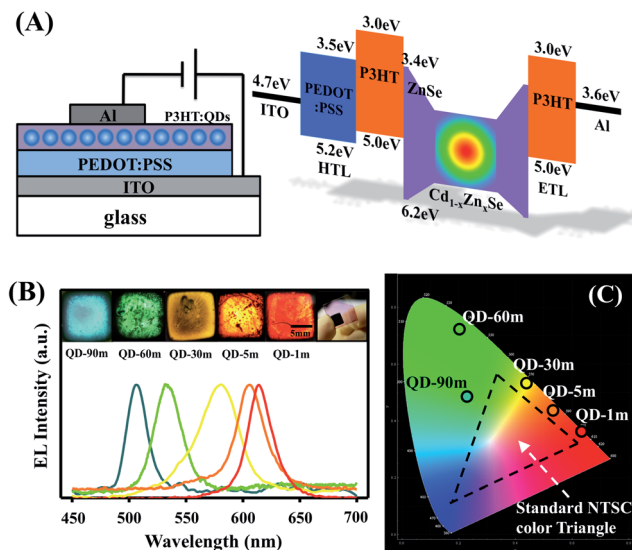|	$A_1/(A_1 + A_2 + A_3)$	τ_1 (ns)	$A_2/(A_1 + A_2 + A_3)$	τ_2 (ns)	$A_3/(A_1 + A_2 + A_3)$	τ_3 (ns)	$\langle\tau\rangle$ (ns)	χ^2
QD-1m	0.29	25.3	0.37	9.6	0.34	2.3	19.0	1.08
QD-15m	0.12	19.4	0.45	6.2	0.43	1.6	10.9	1.10
QD-30m	0.08	12.1	0.34	3.5	0.58	0.9	6.2	1.04
QD-60m	0.05	10.4	0.31	2.6	0.64	0.5	4.7	1.14
QD-90m	0.02	6.9	0.25	1.3	0.73	0.3	2.4	1.01

Fig. 6 (A) Schematic structure of the multilayered QD-LED and the corresponding energy level diagram. (B) EL spectra of QD-LEDs that utilized QD-1m, QD-15m, QD-30m, QD-60m and QD-90m as the active layer. The insets are the EL photographs of the multicolored QD-LEDs and a photograph of the QD-LED prototype. (C) CIE color coordinates of QD-LEDs that utilized QDs with different emission wavelengths.

different colors from red to blue depending on the bandgap energy of the blended QDs. The recorded EL spectra showed Gaussian-shaped peaks with narrow bandwidths similar to the PL spectra of the $Cd_{1-x}Zn_xSe$ QDs, manifesting that the EL of the QD-LEDs mostly originated from the QDs. When the EL spectra were transformed into the CIE color coordinates, they were located outside the standard National Television System Committee (NTSC) color triangle as displayed in Fig. 6(C). This outcome suggests that in a display which integrates the multi-colored QD-LEDs, a significantly larger color triangle on the CIE chromaticity diagram can be acquired.[51,52] The current–voltage characteristics and EL efficiency of the QD-LEDs were also tested. Fig. S7 (ESI)† presents the voltage-dependent variations of current density and EQE for a red emissive QD-LED. A turn-on voltage of about 4.5 V was recorded with a peak EQE of 0.005%, which was comparable to the values attained from the air-operated and unpackaged QD-LEDs.[24,53] It should be noted that further enhancement in EQE could be achieved by optimizing the relevant experimental conditions such as the QD coverage and the thickness of HTL and ETL.[54] Moreover, on increasing the applied voltage, the EL spectra of the QD-LED did not experience obvious spectral shift or peak broadening. This result indicates that exciton polarization induced by a high electric field was effectively prohibited in the tested device,[53] which can be attributed to the screen effect as a result of the core/shell structure of the utilized QDs.[21]

Conclusions

In conclusion, ternary alloyed $Cd_{1-x}Zn_xSe$ QDs with tunable emission wavelengths were successfully synthesized in a single-step hot-injection process by delicately controlling the reaction time. As the reaction progressed, the alloying process extended the bandgap of the $Cd_{1-x}Zn_xSe$ QDs, even though the particle size increased. A type-I core/shell structure was considered for the grown $Cd_{1-x}Zn_xSe$ QDs, which efficiently confined the electrons and holes in the core to provide stable PL. The multicolored $Cd_{1-x}Zn_xSe$ QDs were further utilized to fabricate prototype QD-LEDs that could emit light in tunable and saturated colors, suitable for display applications. The current study demonstrates the versatility of the single-step hot-injection synthesis as well as the potential of the resultant $Cd_{1-x}Zn_xSe$ QDs as promising emitters in solid-state lighting. Further optimization of the structure of the $Cd_{1-x}Zn_xSe$ QDs, for example, by performing a successive shell coating treatment which can significantly enhance the PL quantum yield,[55] may push forward their practical applications in technologically important fields, such as bioanalytics and biolabeling where the stability of PL and its spectral diversity are essential.

References

1 A. P. Alivisatos, *Science*, 1996, **271**, 933–937.
2 W. Zhang, G. Chen, J. Wang, B. C. Ye and X. Zhong, *Inorg. Chem.*, 2009, **48**, 9723–9731.
3 S. Kim, B. Fisher, H. J. Eisler and M. Bawendi, *J. Am. Chem. Soc.*, 2003, **125**, 11466–11467.
4 X. Zhong, R. Xie, Y. Zhang, T. Basch and W. Knoll, *Chem. Mater.*, 2005, **17**, 4038–4042.
5 Z. Deng, H. Yan and Y. Liu, *J. Am. Chem. Soc.*, 2009, **131**, 17744–17745.
6 S. A. Mcdonald, G. Konstantatos, S. Zhang, P. W. Cyr, E. J. D. Klem, L. Levina and E. H. Sargent, *Nat. Mater.*, 2005, **4**, 138–142.
7 S. Jun, E. Jang, J. Park and J. Kim, *Langmuir*, 2006, **22**, 2407–2410.
8 N. Tessler, V. Medvedev, M. Kazes, S. Kan and U. Banin, *Science*, 2002, **295**, 1506–1508.
9 W. U. Hunynh, J. J. Dittmer and A. P. Alivisatos, *Science*, 2002, **295**, 2425–2427.
10 M. J. Panzer, K. E. Aidala, P. O. Anikeeva, J. E. Halpert, M. G. Bawendi and V. Bulović, *Nano Lett.*, 2010, **10**, 2421–2426.
11 M. Bruchez Jr, M. Moronne, P. Gin, S. Weiss and A. P. Alivisatos, *Science*, 1998, **281**, 2013–2016.
12 P. Zrazhevskiy and X. Gao, *Nano Today*, 2009, **4**, 414–428.
13 B. O. Dabbousi, J. Rodriguez-Viejo, F. V. Mikulec, J. R. Heine, H. Mattoussi, R. Ober, K. F. Jensen and M. G. Bawendi, *J. Phys. Chem. B*, 1997, **101**, 9463–9475.

14 Y. Shirasaki, G. J. Supran, M. G. Bawendi and V. Bulović, *Nat. Photonics*, 2013, **7**, 13–23.

15 B. S. Mashford, M. Stevenson, Z. Popovic, C. Hamiltion, Z. Zhou, C. Breen, J. Steckel, V. Bulović, M. Bawendi, S. Coe-Sullivan and P. T. Kazlas, *Nat. Photonics*, 2013, **7**, 407–412.

16 K.-J. Chen, H.-C. Chen, K.-A. Tsai, C.-C. Lin, H.-H. Tsai, S.-H. Chien, B.-S. Cheng, Y.-J. Hsu, M.-H. Shih, C.-H. Tsai, H.-H. Shih and H.-C. Kuo, *Adv. Funct. Mater.*, 2012, **22**, 5138–5143.

17 S. Jun and E. Jang, *Angew. Chem.*, 2013, **125**, 707–710.

18 B. N. Pal, I. Robel, A. Mohite, R. Laocharoensuk, D. J. Werder and V. I. Klimov, *Adv. Funct. Mater.*, 2012, **22**, 1741–1748.

19 X. Yang, D. Zhao, K. S. Leck, S. T. Tan, Y. X. Tang, J. Zhao, H. V. Demir and X. W. Sun, *Adv. Mater.*, 2012, **24**, 4180–4185.

20 S. Kim, S. H. Im and S.-W. Kim, *Nanoscale*, 2013, **5**, 5205–5214.

21 K.-H. Lee, J.-H. Lee, W.-S. Song, H. Ko, C. Lee, J.-H. Lee and H. Yang, *ACS Nano*, 2013, **7**, 7295–7302.

22 H. Shen, S. Wang, H. Wang, J. Niu, L. Qian, Y. Yang, A. Titov, J. Hyvonen, Y. Zheng and L. S. Li, *ACS Appl. Mater. Interfaces*, 2013, **5**, 4260–4265.

23 H.-S. Chen, K.-W. Wang, S.-S. Chen and S.-R. Chung, *Opt. Lett.*, 2013, **38**, 2080–2082.

24 V. L. Colvin, M. C. Schlamp and A. P. Alivisatos, *Nature*, 1994, **370**, 354–357.

25 S. Coe, W. K. Woo, M. Bawendi and V. Bulović, *Nature*, 2002, **420**, 800–803.

26 Q. Sun, Y. A. Wang, L. S. Li, D. Wang, T. Zhu, J. Xu, C. Yang and Y. Li, *Nat. Photonics*, 2007, **1**, 711–722.

27 P. O. Anlkeeva, J. E. Halpert, M. G. Bawendi and V. Bulović, *Nano Lett.*, 2009, **9**, 2532–2536.

28 J. Kwak, W. K. Bae, D. Lee, I. Park, J. Lim, M. Park, H. Cho, H. Woo, D. Y. Yoon, K. Char, S. Lee and C. Lee, *Nano Lett.*, 2012, **12**, 2362–2366.

29 W. K. Bae, J. Kwak, J. Lim, D. Lee, M. K. Nam, K. Char, C. Lee and S. Lee, *Nano Lett.*, 2010, **10**, 2368–2373.

30 M. D. Regulacio and M. Y. Han, *Acc. Chem. Res.*, 2010, **43**, 621–630.

31 X. Zhong, M. Han, Z. Dong, T. J. White and W. Knoll, *J. Am. Chem. Soc.*, 2003, **125**, 8589–8594.

32 D. Chen, F. Zhao, H. Qi, M. Rutherfold and X. Peng, *Chem. Mater.*, 2010, **22**, 1437–1444.

33 A. Maliakal, H. Katz, P. M. Cotts, S. Subramoney and P. Mirau, *J. Am. Chem. Soc.*, 2005, **127**, 14655–14662.

34 (*a*) T. Pons, H. T. Uyeda, I. L. Medintz and H. Mattoussi, *J. Phys. Chem. B*, 2006, **110**, 20308–20313; (*b*) A. M. Smith and S. Nie, *J. Am. Chem. Soc.*, 2011, **133**, 24–26; (*c*)

C. M. Evans, L. Guo, J. J. Peterson, S. Maccagnano-Zacher and T. D. Krauss, *Nano Lett.*, 2008, **8**, 2896–2899.

35 (*a*) V. I. Klimov, *J. Phys. Chem. B*, 2000, **104**, 6112–6123; (*b*) H. Lee, P. H. Holloway, H. Yang, L. Hardison and V. D. Kleiman, *J. Chem. Phys.*, 2006, **125**, 164711.

36 (*a*) A. M. Brouwer, *Pure Appl. Chem.*, 2011, **83**, 2213–2228; (*b*) Y.-J. Hsu and S.-Y. Lu, *Langmuir*, 2004, **20**, 194–201; (*c*) Y. Zheng, Z. Yang and J. Y. Ying, *Adv. Mater.*, 2007, **19**, 1475–1479.

37 A. P. Alivisatos, *J. Phys. Chem.*, 1996, **100**, 13226–13239.

38 X. Zhong, Y. Feng, W. Knoll and M. Han, *J. Am. Chem. Soc.*, 2003, **125**, 13559–13563.

39 S. A. Santangelo, E. A. Hinds, V. A. Vlaskin, P. I. Archer and D. R. Gamelin, *J. Am. Chem. Soc.*, 2007, **129**, 3973–3978.

40 B. Blackman, D. Battaglia and X. Peng, *Chem. Mater.*, 2008, **20**, 4847–4853.

41 B. Blackman, D. M. Battaglia, T. D. Mishima, M. B. Johnson and X. Peng, *Chem. Mater.*, 2007, **19**, 3815–3821.

42 D. Battaglia, B. Blackman and X. Peng, *J. Am. Chem. Soc.*, 2005, **127**, 10889–10897.

43 S. Sadhu and A. Patra, *J. Phys. Chem. C*, 2012, **116**, 15167–15173.

44 J. A. Mgguire, J. Joo, J. M. Pietryga, R. D. Schaller and V. I. Klimov, *Acc. Chem. Res.*, 2008, **41**, 1810–1819.

45 F. García-Santamaría, Y. Chen, J. Vela, R. D. Schaller, J. A. Hollingsworth and V. I. Klimov, *Nano Lett.*, 2009, **9**, 3482–3488.

46 T. R. Cundari and W. Fu, *Int. J. Quantum Chem.*, 1999, **71**, 47–56.

47 H. Lee, H. Yang and P. H. Holloway, *J. Lumin.*, 2007, **126**, 314–318.

48 L. S. Li, N. Pradhan, Y. Wang and X. Peng, *Nano Lett.*, 2004, **4**, 2261–2264.

49 S. A. Choulis, Y. Kim, J. Nelson and D. D. C. Bradley, *Appl. Phys. Lett.*, 2004, **85**, 3890–3892.

50 D. Wakizaka, T. Fushimi, H. Ohkita and S. Ito, *Polymer*, 2004, **45**, 8561–8565.

51 J. S. Steckel, P. Snee, S. Coe-Sullivan, J. P. Zimmer, J. E. Halpert, P. Anikeeva, L.-A. Kim, V. Bulovic and M. G. Bawendi, *Angew. Chem., Int. Ed.*, 2006, **45**, 5796–5799.

52 W. K. Bae, J. Kwak, J. W. Park and K. Char, *Adv. Mater.*, 2009, **21**, 1–5.

53 V. Wood, M. J. Panzer, J.-M. Caruge, J. E. Halpert, M. G. Bawendi and V. Bulović, *Nano Lett.*, 2010, **10**, 24–29.

54 Q. Sun, Y. A. Wang, L. S. Li, D. Wang, T. Zhu, J. Xu, C. Yang and Y. Li, *Nat. Photonics*, 2007, **1**, 717–722.

55 B. C. Fitzmorris, Y.-C. Pu, J. K. Cooper, Y.-F. Lin, Y.-J. Hsu, Y. Li and J. Z. Zhang, *ACS Appl. Mater. Interfaces*, 2013, **5**, 2893–2900.